Characterization of CdxPb1-xS thin films

Characterization of CdxPb1-xS thin films

4.1 Introduction

The need of new and improved optical and electrical properties has stimulated the study of thin solid films of elements, binary and ternary system, with controlled composition and specific properties [1-6]. The preparation and application of thin films plays an important role in the present context of energy crisis. Thin films prepared by different methods show different physical and chemical properties. This means that the properties of the film are methodology dependent [7-12].

Among the different deposition techniques, the chemical bath deposition is a simple, convenient, low temperature, for growth of thin films. To know the different properties of the film, it is necessary to characterize the film by using various characterization techniques. The techniques which are used for characterization of thin films are thickness measurement, X-ray diffraction (XRD). Atomic absorption spectroscopy (AAS), optical absorption measurement, electrical conductivity, thermo-electrical studies and scanning electron microscopy etc.

The most important aspect of characterization contains the identification of structure compositional analysis, optical band gap, etc. The crystal structure of thin film was well understood by XRD. From XRD data lattice parameters, crystallite size, unit cell dimensions of the material can be measured. SEM characterizes the size, shape and mutual arrangement of individual crystal grains. However the optical property measurements give information regarding the optical band gap and nature of optical transitions. The information regarding the electrical properties has been found to depend on different parameter like deposition rate, substrate temperature etc.

The chapter gives the details of growth mechanism structural, compositional, optical and morphological analysis, electrical analysis of the $Cd_xPb_{1-x}S$ thin films.

4.2 Growth mechanism

A solid state material formation involves two main possible reactions.

1. Homogenous precipitation within the bulk of solution [13-14]

2. Heterogeneous precipitation, at the interface of the substrate.

The deposition of thin film occurs in two distinct mechanisms i.e. ion-by-ion or cluster-by-cluster mechanism [15-19]. In ion-by-ion mechanism the ions condense at the reacting surface to form the film. In cluster mechanism agglomeration of colloidal particles in solution occurs by homogenous reaction. The ion-by-ion growth results in the thin, uniform and adherent films. When ionic product of metal ion and chalcogenide ion exceeds the solubility product, the formation of film takes place, as the solution becomes supersaturated.

For deposition of $Cd_xPb_{1-x}S$ thin films, an alkaline bath was prepared by mixing cadmium sulphate, lead acetate, Na_2EDTA, ammonia, potassium hydroxide and thiourea. It was noted that a clear solution is obtained at 300K. The metal ions are in complexed state [M(A)n]. Low temperature lowers kinetic energy of the ions and avoids the precipitation. The release of ions by the complexing species is a thermally activated process [20]. The increase in temperate results in dissociation of the complex, releasing metal ions, to be incorporated as an alloy in the form of thin film.

The growth mechanism of film can be understood from the following reactions,

$$NH_2\text{-}CS\text{-}NH_2 + OH^- \longrightarrow NH_2\text{-}CO\text{-}NH_2 + Na_2SO_4 + HS^- \quad (4.1)$$

$$HS^- + OH^- \longrightarrow S^{2-} + H_2O \quad (4.2)$$

$$X[(Cd(EDTA)_n] + (1-x)\,[Pb\,(EDTA)_n] + S^{2-} \longrightarrow Cd_xPb_{1-x}S + 2nEDTA. \quad (4.3)$$

The film formation takes place by the recombination of the ions on the substrate surface via nucleation followed by growth process. In case of pseudo binary cadmium chalcogenide thin films, $Cd(OH)_2$ is considered as seeding nude us [21-25]. However, in case of $Cd_xPb_{1-x}S$ no initial white layer of $Cd(OH)_2$ was observed but instead a black layer was noted. Since the solubility product of PbS is lower than that of CdS, increase in temperature free Pb^{+2} ions increases, which combine with S^{2-} ions on the substrates than Cd^{+2} ions yielding an initial black layer of PbS was noted

[26]. Since the solubility product of PbS is lower than that of CdS, increase in temperature makes free Pb^{2+} ions from complexed state, which combines with S^{-2} ions on the substrate than Cd^{+2} ions yielding an initial black layer of PbS. The layer act as catalyst for further growth of film. Thus formed layer grows further by adsorbing more and more Cd^{+2}, Pb^{2+} and S^{-2} ions to form ternary $Cd_xPb_{1-x}S$ thin films.

It is found that the rate of deposition of the films depends on the degree of supersaturation, temperature of bath, and pH of solution. Thus lower the super saturation, slower is the formation of MS material. If the concentration of OH^- ion is more in the solution, the concentration of M^{+2} ion is small resulting in lower super saturation value and thus slow rate of reaction. As we increase the pH of solution the concentration of Pb^{+2} ions decreases that results in decrease in the rate of film formation. The nucleation is not observed within the first thirty minutes and hence it can be inferred that the process requires an induction period for nucleation on the substrate.

In order to optimize depositional temperature to get good quality, better thickness film, the experiments were carried out at various temperatures (273K to 373K). Figure (4.1a) shows variation of thickness with temperature. From figure it can be seen that film with better thickness can be obtained at 343K. Therefore this optimized condition was used for the growth of all films. The optimization of deposition time of film was carried out in the same manner. Figure (4.1b) shows alteration in thickness with time for a typical $Cd_{0.5}Pb_{0.5}S$ thin film at 343K. From figure, it is observed that thickness varies quasilinearly with time. The thickness was observed to saturate after a deposition time of 180 minutes. Films obtained were well adherent to glass substrate and homogenous. All the films were deposited for 180 minutes with constant rotation speed of 45± 2rpm. If the speed of rotation is increased beyond this speed, thick films were obtained. Thus optimized conditions for obtaining good quality thin films are

maintaining pH 10.5± 0.2, speed of rotation 45± 2, temperature 343K and deposition time of 180 minutes.

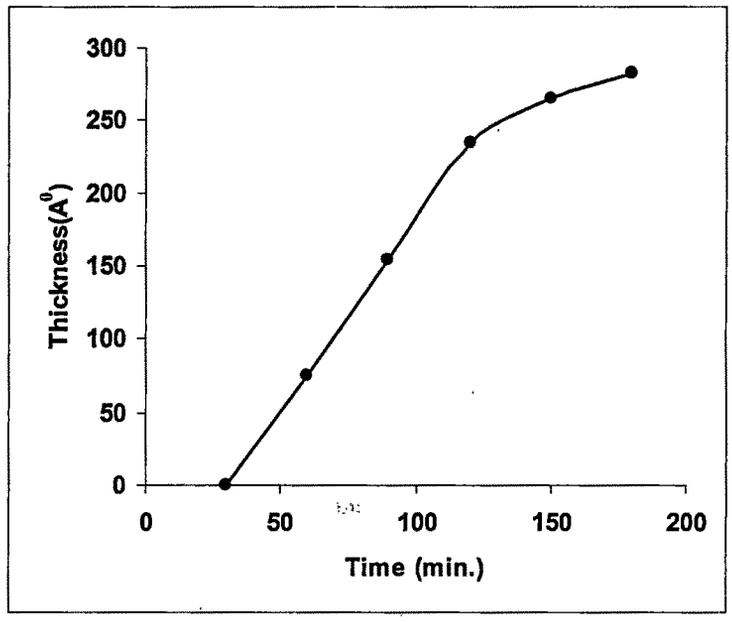

Fig 4.1(a)

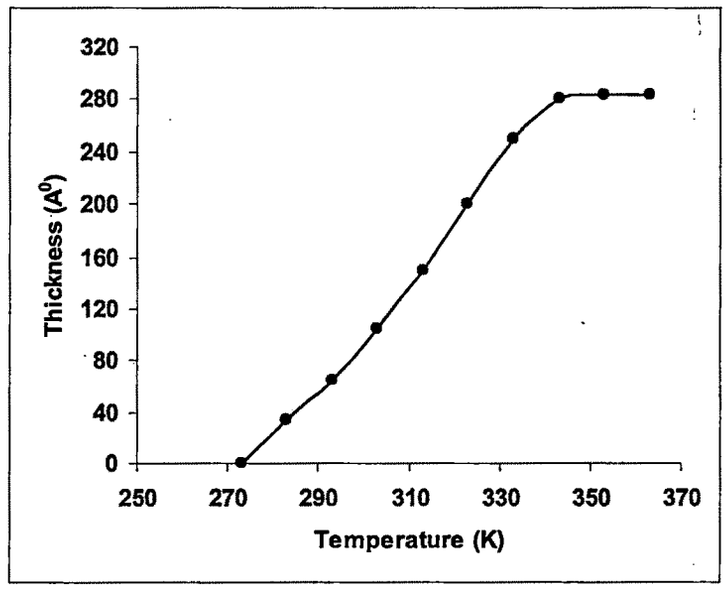

Fig 4.1(b)

Fig 4.1: Growth mechanism of representative $Cd_{0.5}Pb_{0.5}S$ thin films.

a) A plot of thickness against deposition time at 343K

b) A plot of thickness against temperature for 180 minutes

4.3 Thickness measurement

The terminal thickness of films has been measured by weight difference density consideration method. The formula used was;

$$t = m/l.b.d \qquad (4.4)$$

Where t is thickness of film, l is length of film, b is the breadth of film and d is the density. For CdS 4.82 g/cc and for PbS 7.5 g/cc density was used. The values of thickness so obtained are given in Table along with other data. The non-linear variation of thickness with composition parameter (x) was observed. The films obtained were uniform, well adherent to the substrate and homogenous. The as grown films of PbS were black in colour while that of CdS were yellow in colour [27-31]. As the composition parameter 'x' increases the colour of film changes from black to yellow due to substitution of Pb^{+2} by Cd^{+2} in the lattice of PbS. The thickness of film was found to be 234 Å for PbS film and for CdS was 209Å.

4.4 Compositional Analysis

The composition of cadmium and lead in the sample were determined by atomic absorption studies. A Perkin-Elmer 3030, Atomic absorption spectrophotometer was used for this purpose. The weighted film sample was dissolved in minimum quantity of concentrated AR grade HNO_3. The products obtained are as shown below.

$$CdS + 2HNO_3 \longrightarrow Cd(NO_3)_2 + S^{2-} + H_2O \qquad (4.5)$$

$$PbS + 2HNO_3 \longrightarrow Pb(NO_3)_2 + S^{2-} + H_2O \qquad (4.6)$$

The filtrate containing nitrates of cadmium and lead were diluted to appropriate concentration and determined by using AAS. The standard solutions used for plotting calibration curve were prepared by diluting commercial standards to concentration 0.4, 0.8, 1.2, 1.6, 2.0 μg/ml for cadmium and 0.4, 0.8, 1.6, 2.0 μg/ml for lead. The ratio of [Pb/Cd] ion concentration in the films were calculated, which matches with the ions concentration taken in bath. The concentrations and ratio of [Pb/Cd] obtained by measurements are shown in the Table 1. It is observed that the ratio of Pb and Cd concentration taken in bath during deposition of films

was roughly the same as entered in film. Therefore it can be concluded that the films formed are of better stiochiometry.

4.5 Structural and Morphological Investigation

Structural analysis was done by observing the XRD pattern, recorded by Philips PW-1710 (Holland) X-ray diffractometer in 2θ range from 10^0-80^0 using Cukα line (λ = 1.54056 A^0). The X-ray diffraction (XRD) spectra of annealed $Cd_xPb_{1-x}S$ thin films deposited on glass substrate are shown in fig. (4.2 a-e). The sulphide of cadmium can be formed with either hexagonal or cubic structure and sulphide of Pb can be formed with cubic structure. In the present investigation we obtained a large number peaks for each time indicating these polycrystalline nature.

The deposits are polycrystalline over whole range of the parameter x ($0 \leqslant x \leqslant 1$) studied. Pure PbS is the cubic type and the intense reflections have been observed at 2.096, 2.965 and 3.420 Å, while for hexagonal CdS at 3.483, 3.357, 3.60 Å [32-33]. The X-ray diffractogram of all samples have also been analyzed. The standard pattern of cubic PbS and hexagonal CdS are displayed in Table 2 for comparison purpose. It has been observed that for films with $0 \leqslant x \leqslant 0.4$ solid solution of the kind $Cd_xPb_{1-x}S$ have been formed and are of cubic type. The most intense peak corresponds to (200) reflection shifts towards lower d values with a corresponding decrease in relative intensity.

The lattice parameter 'a' is calculated from these observations and found to b decreased with increase in 'x' upto 0.4. The variation of 'a' with 'x' is linear. For higher values of 'x' ($x \geqslant 0.5$) more abrupt change is observed which can be ascribed to the formation of individual phases. Beyond 0.4 ($0.5 \leqslant x \leqslant 1$), sample consist of mixture of separate phases of cubic PbS and hexagonal CdS.

The hexagonal phase of CdS is little bit increased as 'x' is increased from 0.5 to 1. The lattice constants fit well with their ASTM data. This clearly indicates that the thin films deposited for various 'x' values (0.5 to 1)

are mixtures or composites of the type $(CdS)_x(PbS)_{1-x}$ and not to be $Cd_xPb_{1-x}S$ ($0.5 \leqslant x \leqslant 1$) solid solutions.

These observations are similar to those reported by Deshmukh et al [34]. The diffractogram of CdS (fig. 4.2e) contains most intense peak corresponding to (002) reflection of hexagonal phase .However ASTM data shows the (101) as the most intense reflection for hexagonal phase. Thus in our case instead of (101), (002) reflection is of highest intensity. Again if hexagonal phase exists with basal plane orientation as (002) reflection plane parallel to the substrate surface, (002) reflection will have higher intensity. Thus it is inferred that deposits are hexagonal in phase .For Pb incorporated films ($0.5 \leqslant x \leqslant 0.9$) prominent peaks occur at same positions that for pure CdS, indicating no appreciable shift in 2θ values. Further the XRD also shows peaks belonging to cubic PbS this weakens the possibility of formation of solid solution of CdS and PbS. For composition x between 0.5 to 0.9 CdS (H) peak intensity increases while PbS (C) peak intensity decreases .As the peak width of CdS (H) changes for composition x. 0.4, it is concluded that the Pb may be acting, as dopant to little extent in CdS [35].

The various crystallographic parameters obtained for all the films are displayed in Table 2 and 3. The observed peak pattern along with their corresponding hkl planes are shown in Table 2. While Table 3 displays the lattice parameter and grain size of all the films. Calculation of grain size was done using Scherrer's relation. The grain size changes roughly from 234 Å to 600 Å as 'x' is varied from 0 to 1.

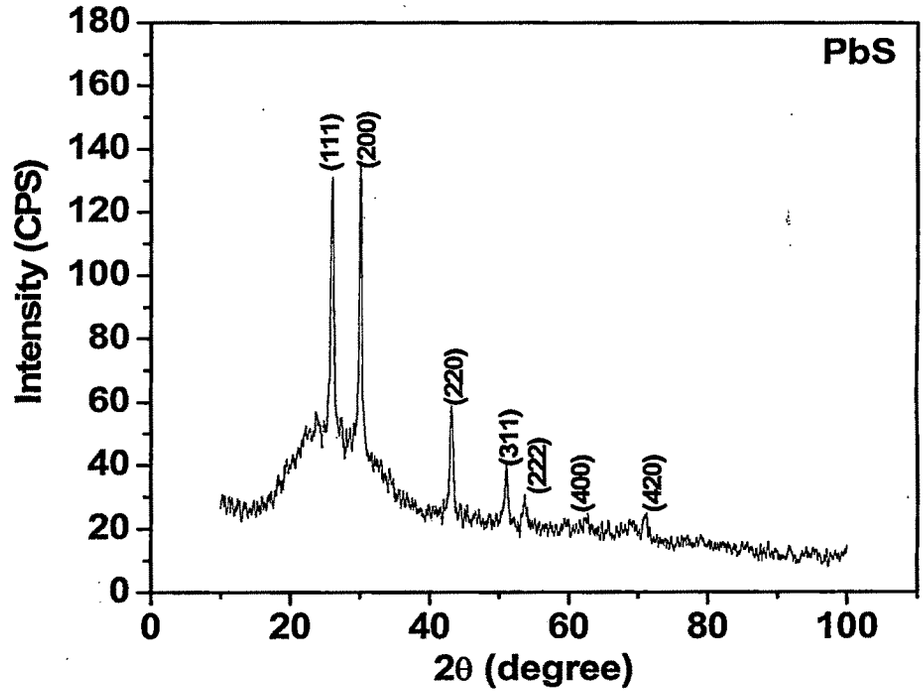

Fig 4.2 (a)

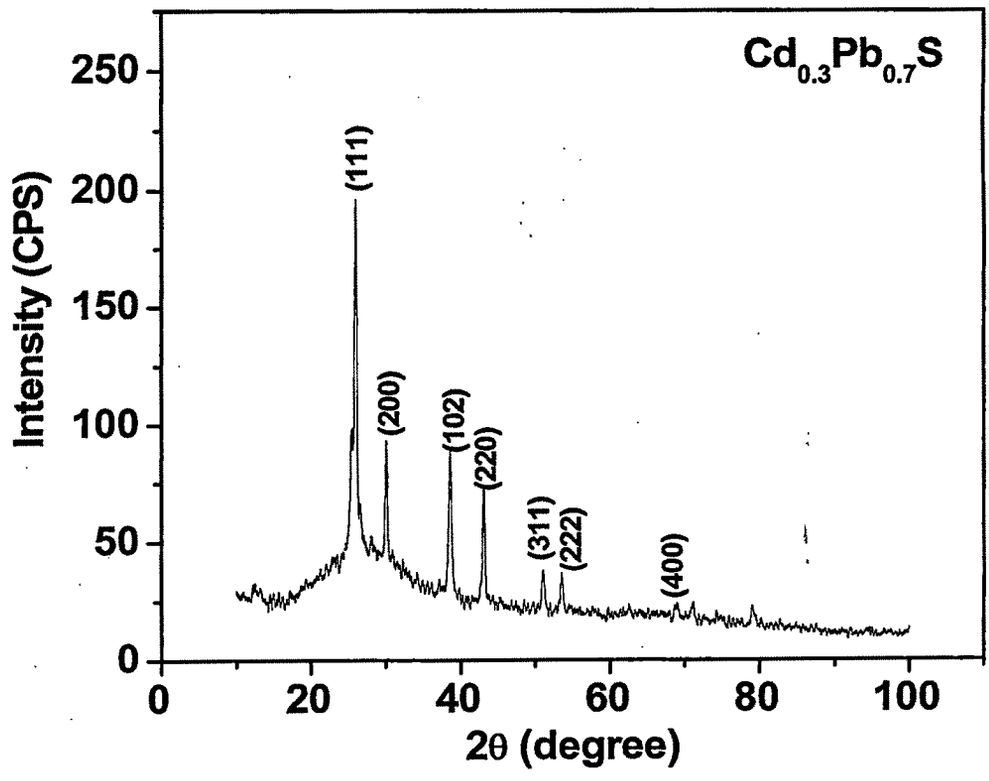

Fig 4.2 (b)

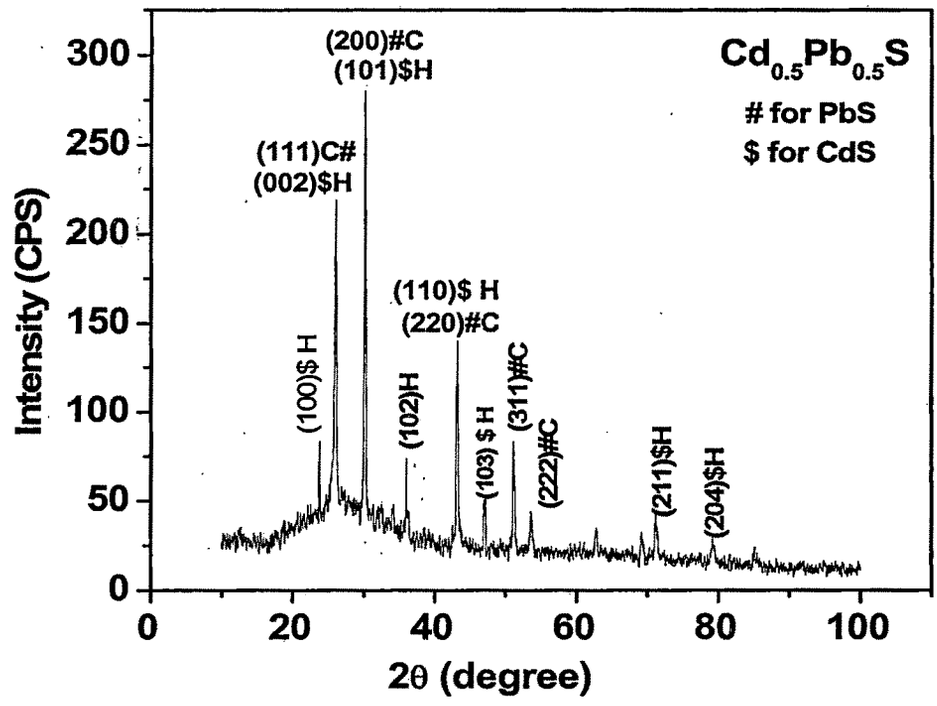

Fig 4.2(c)

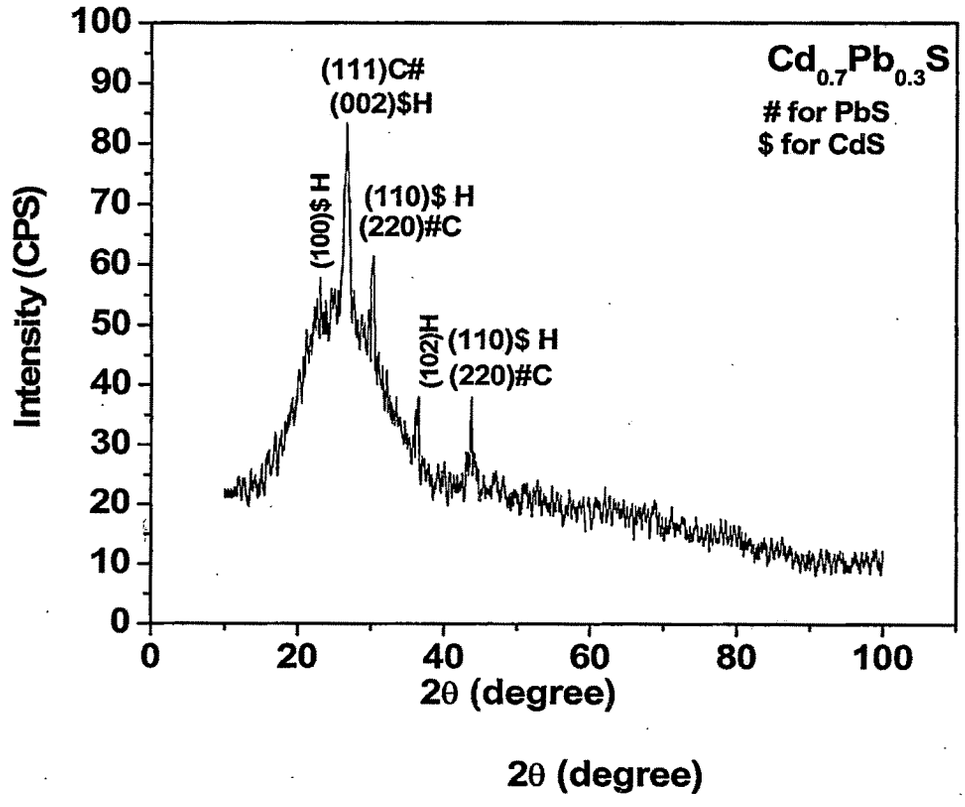

Fig 4.2 (d)

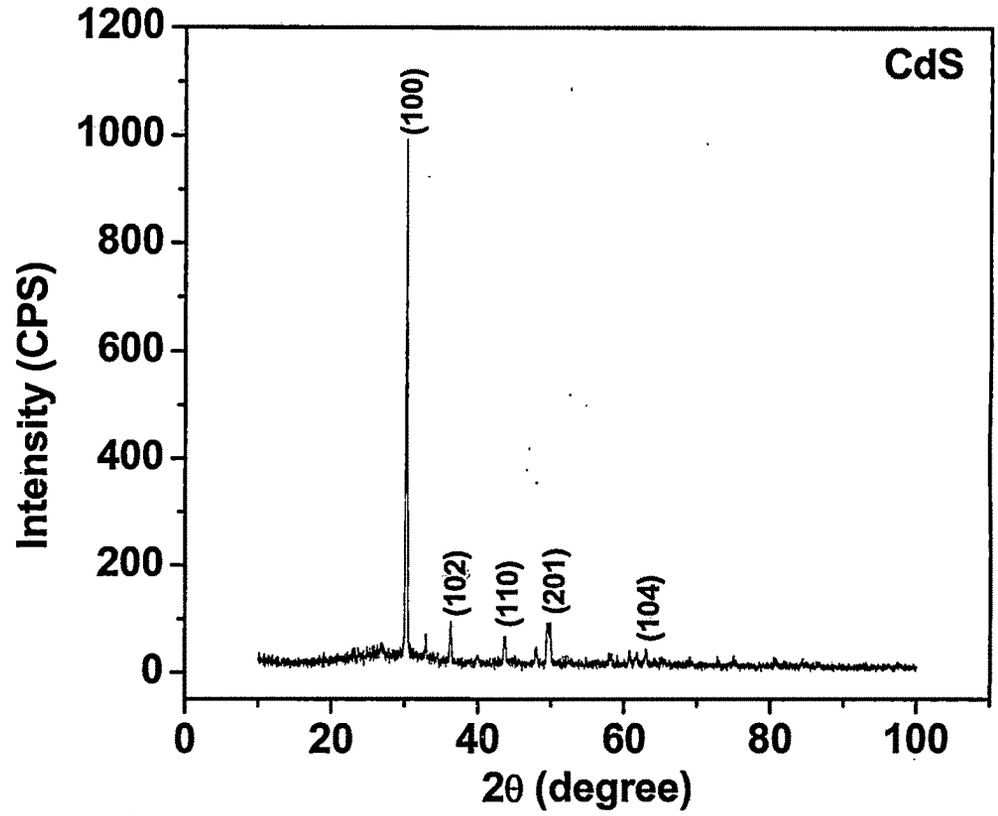

Fig 4.2 (e)

Fig 4.2 XRD pattern of 'annealed' $Cd_xPb_{1-x}S$ thin films

a) x = 0.0, b) x = 0.3, c) x = 0.5, d) x = 0.7, e) x = 1.0

Morphological studies were carried out by using scanning election microscopy. The SEM photographs of all the films $Cd_xPb_{1-x}S$ samples are shown in fig (4.3a-h). $Cd_xPb_{1-x}S$ thin films are homogenous, crack free and uniform. The grains for films with composition $0.0 \leqslant x \leqslant 0.4$ are found to be almost of similar size, this might be due to formation of a single solid solution phase, while variable size grains are observed for films with $0.5 \leqslant x \leqslant 1$ composition.

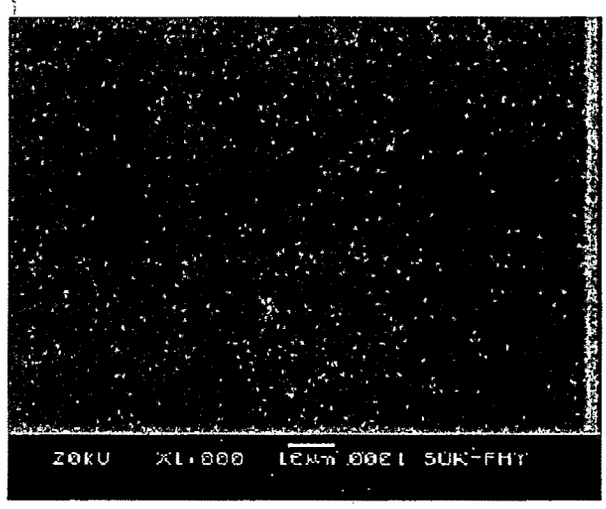

(a) x= 0.0

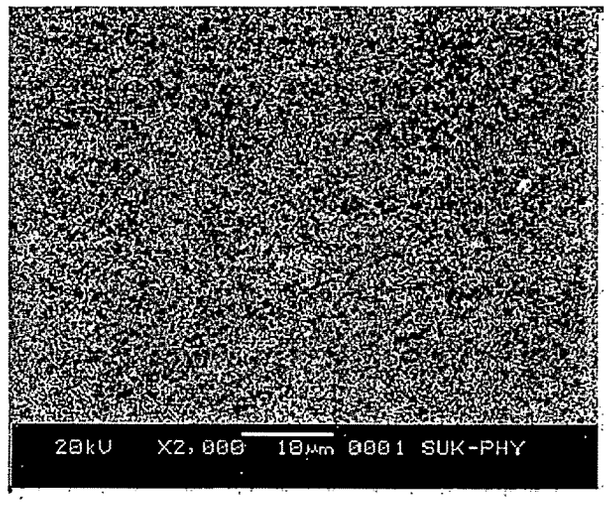

(b) x=0.1

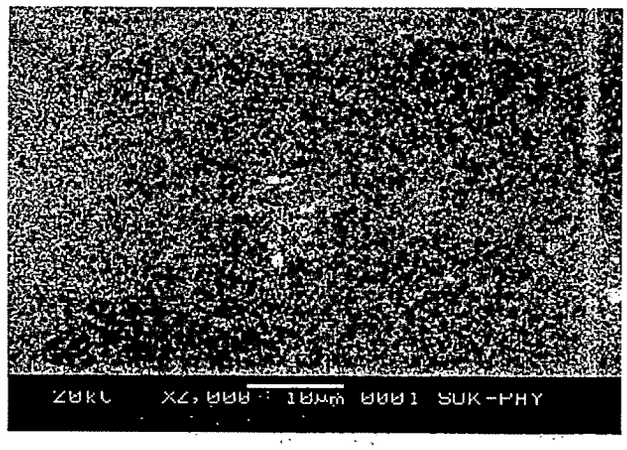

(c) x=0.3

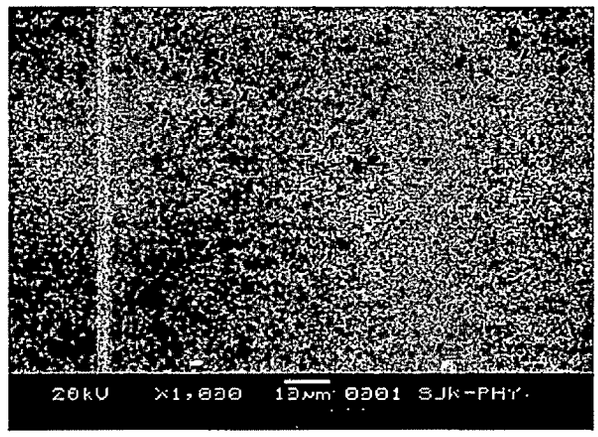

(d) x=0.4

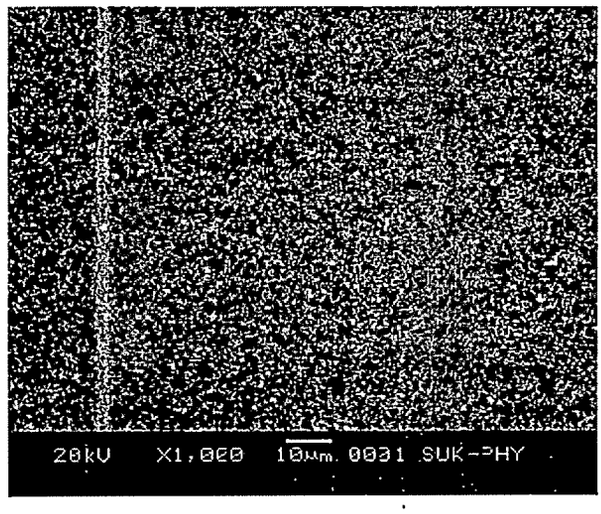

(e) x= 0.5

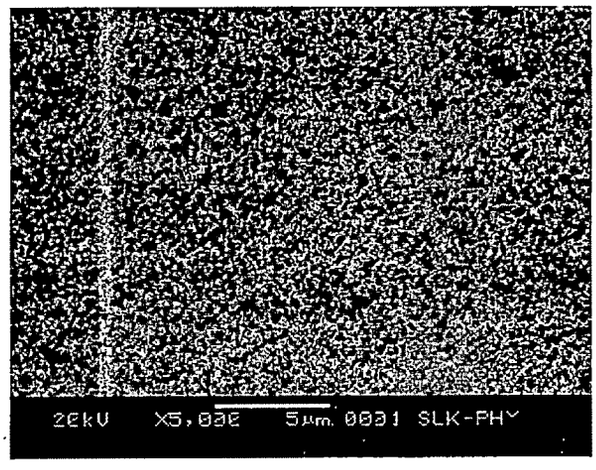

(f) x= 0.7

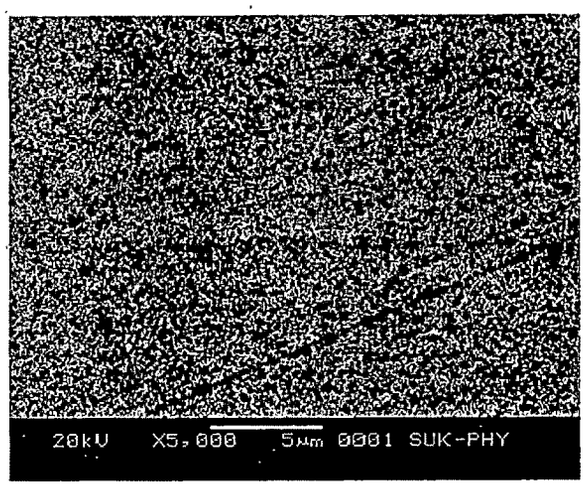

(g) =0.9

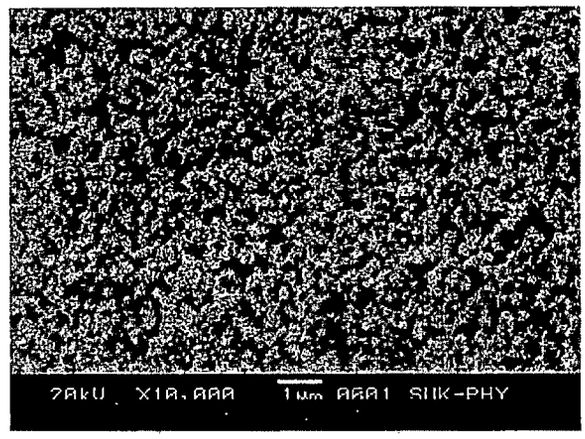

(h) x=1.0

Fig 4.3: SEM micrographs of chemically deposited $CdxPb_{1-x}S$ thin films for cadmium content, (a) x=0.0, (b) x=0.1, (c) x=0.3, (d) x=0.4, (e) x=0.5, (f) x=0.7, (g) x=0.9, (h) x= 1.0

4.6 Optical properties

The optical absorption spectra of various $Cd_xPb_{1-x}S$ films deposited onto glass substrate were studied in the wavelength range of 400 nm to 1600 nm. The spectra were utilized for calculation of absorption coefficient (α), nature of transition involved and band gap. The optical absorption spectra of few representative films are shown in fig (4.4a & b), the spectra shows two regions one for higher wavelength and other for lower wavelength.

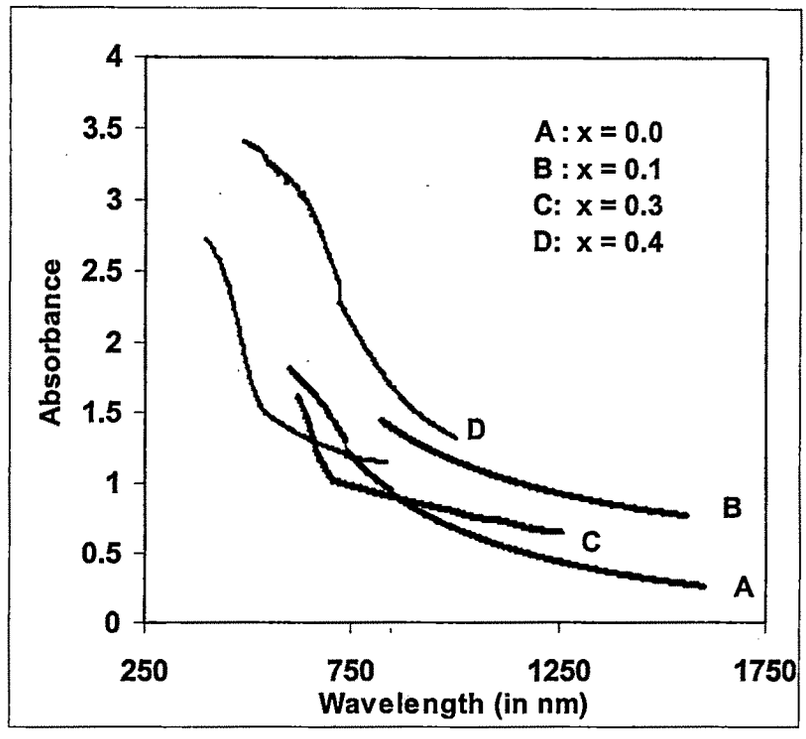

Fig 4.4(a)

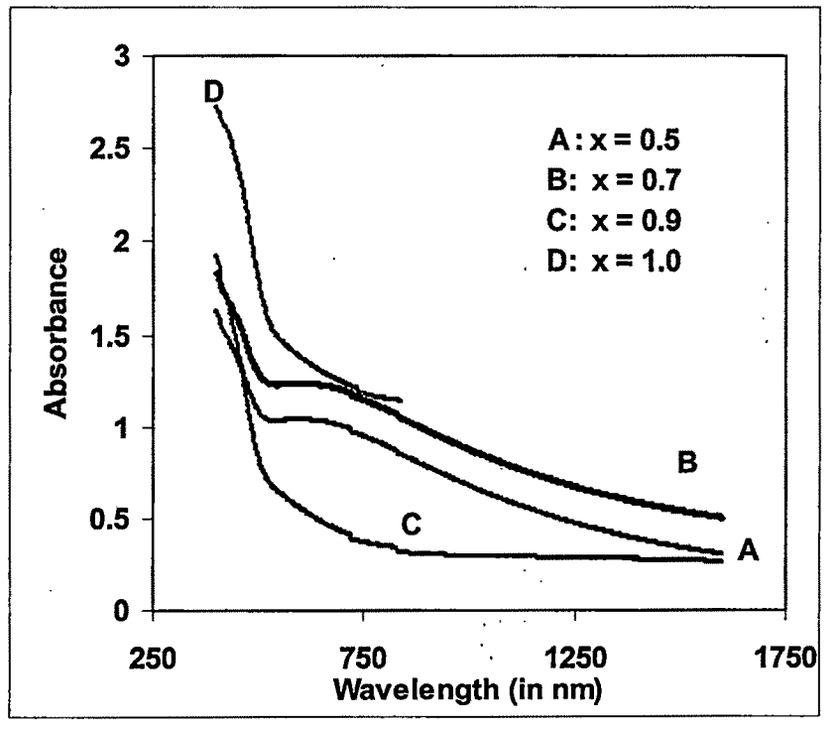

Fig 4.4(b)

Fig 4.4: Absorption spectra of chemically deposited $CdxPb_{1-x}S$ thin films

As the Cd content increases in PbS, the absorption shows a decreasing trend. This is due to wider band gap of CdS. The dependence of absorption coefficient with band gap is given by,

$$\alpha h\nu = A\,(h\nu - Eg)^n \qquad (4.7)$$

Where, A is absorption coefficient (cm^{-1}), hν is photon energy (eV), Eg is the band gap, n is a pure number. For direct type of transitions, the plot of $(\alpha h\nu)^2$ versus hν should be straight line whose intercept to the X-axis gives the optical band gap. Accordingly $(\alpha h\nu)^2$ versus hν plots for few of the representative samples are shown in fig (4.5 a-f). Band gap of PbS and CdS were found to be 0.9 eV and 2.4 eV respectively, which matches well with reported values [36-37]. The band gap increases as the composition parameter 'x' increases from 0.0 to 0.4. While for films with composition $0.4 \leqslant x \leqslant 1$, two band gaps were observed corresponding to individual phases of CdS and PbS. The values of band gap for different composition are listed in Table 4.

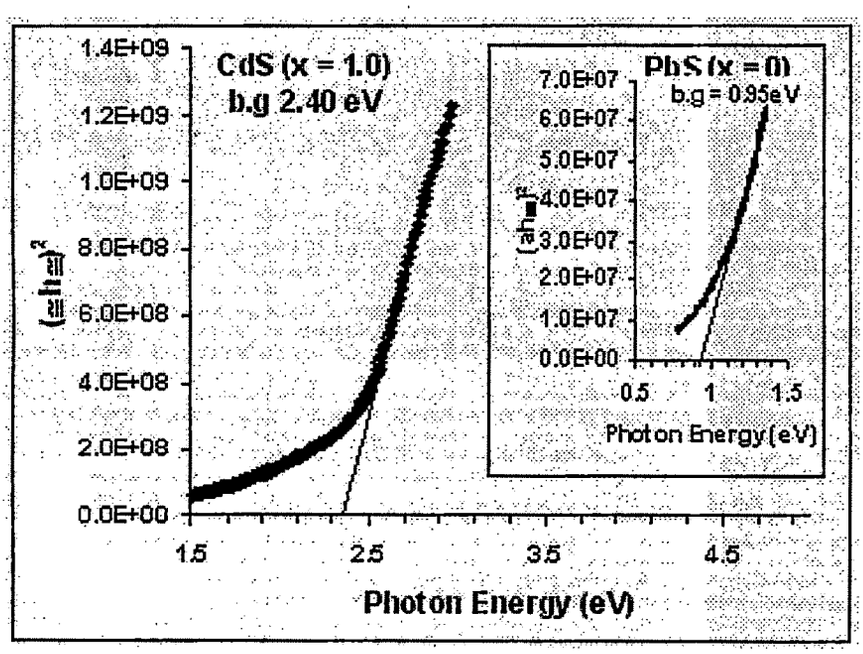

Fig 4.5a: Calculation of Band gap for CdS (x = 1.0) and PbS (x = 0)

BALASAHEB KHARDEKAR LIBRARY
SHIVAJI UNIVERSITY, KOLHAPUR.

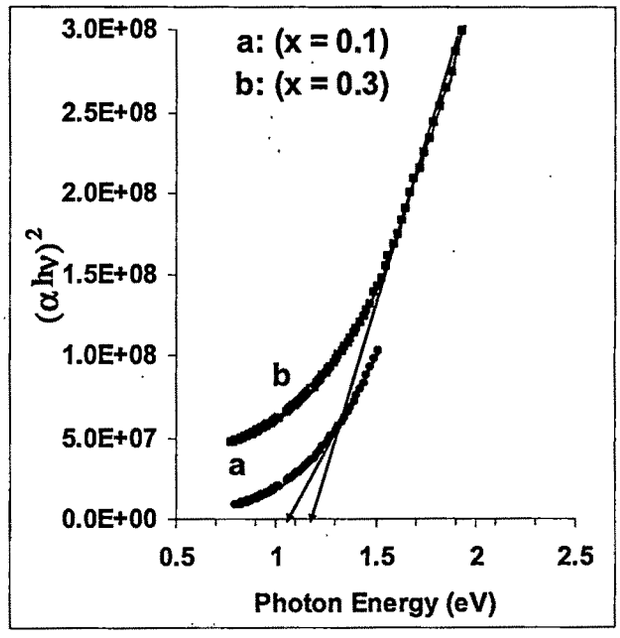

Fig 4.5b:(Band gap for x = 0.1 [a] & x = 0.3 [b])

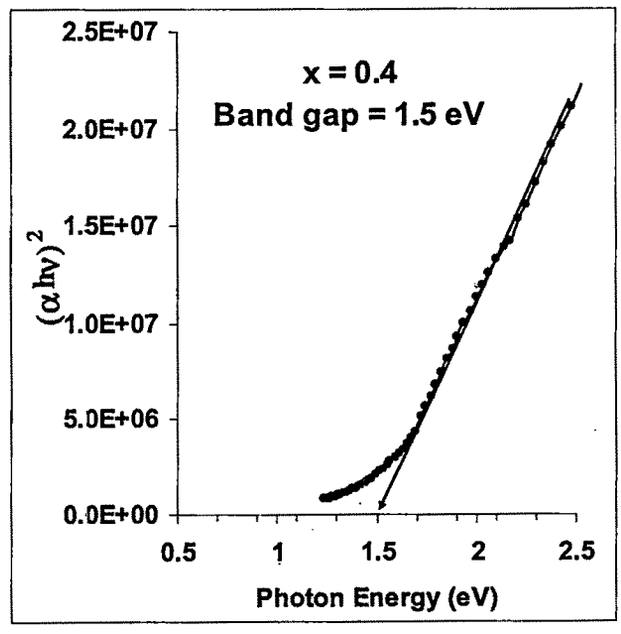

Fig 4.5c:(Calculation of Band gap for x = 0.4)

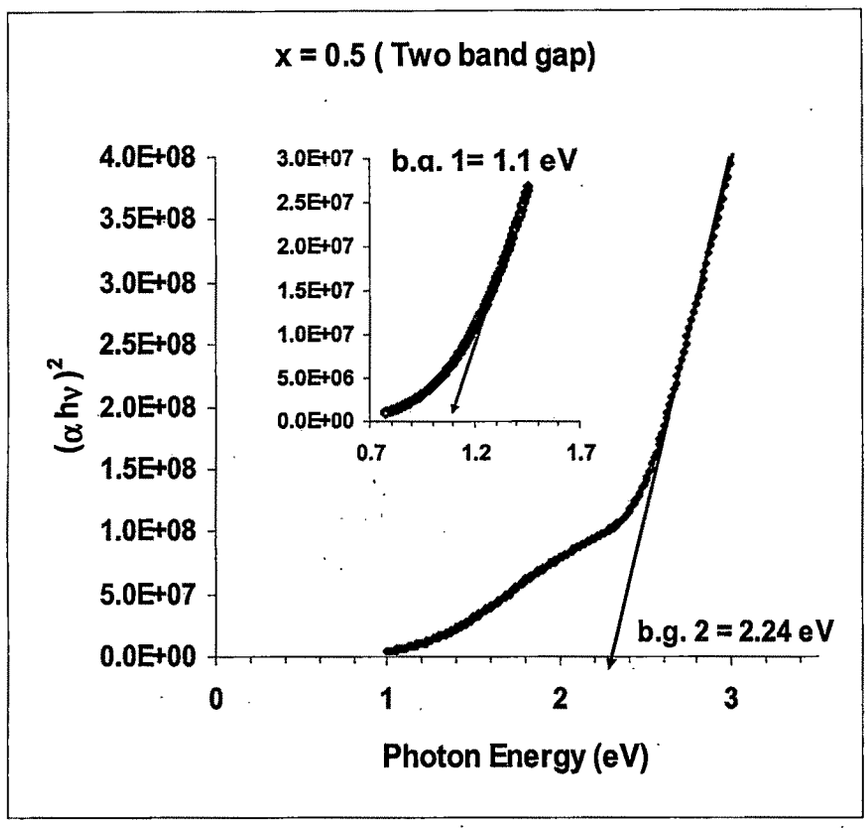

Fig 4.5d: (Calculation of Band gaps for x = 0.5)

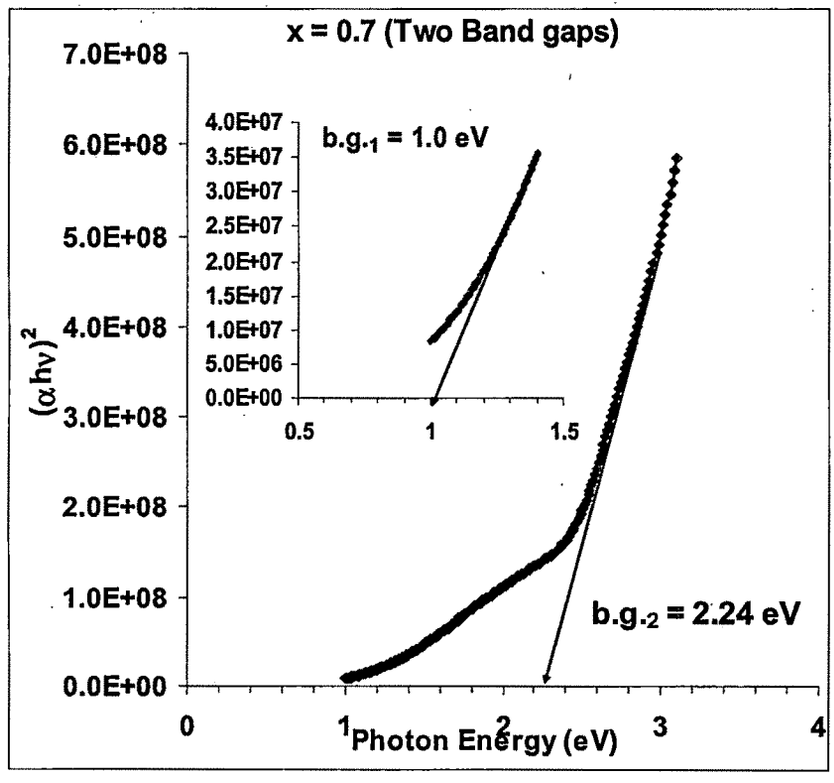

Fig 4.5e: (Calculation of Band gaps for x = 0.7)

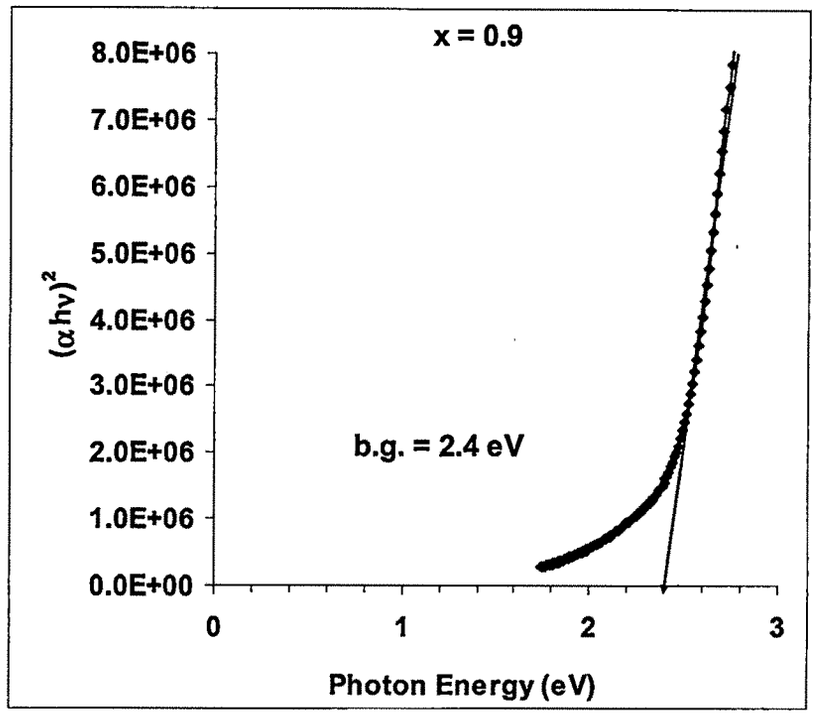

Fig 4.5f: (Calculation of Band gaps for x = 0.9)

4.7 Electrical Properties

The electrical properties are important as they determine the quality and applications of semiconductor devices.

4.7.1 Electrical conductivity

The D.C. conductivity of all the samples was measured by using two probe method, in temperature range 300-500K. For a semiconductor the electrical conductivity. The electrical conductivity at higher temperature is due to thermally generated vacancies of ions (the intrinsic type of conductivity). At low temperature, the thermal energy generated is just sufficient to allow the migration of charge carriers into the vacancies (called extrinsic conductivity) [38-39]. The electrical activation energy is calculated by using Arrhenius equation

$$\sigma = \sigma_0 \exp(-Ea/kT) \qquad (4.8)$$

Where σ is the conductivity, σ_0 is the constant, Ea is the energy of activation, k is Boltzmann constant and T is the absolute temperature. Fig (4.6a to k) shows the plots of log σ versus 1000/T for all the films. The graphs show the presence of two conduction mechanism viz intrinsic and extrinsic. The trend

of decrease in electrical conductivity may be due to widening of band gap and decrease of grain size with increase in composition parameter 'x'. The activation energies calculated from the slope of straight lines of log σ vs. 1000/T plots are given in table. The values were found to be between 0.035 eV to 0.600 eV. The values obtained for activation energy well matches with previously reported values for PbS and CdS [34].

The values of specific conductance at different composition are listed in table. The dark specific conductance of PbS and CdS thin film was found to be 1.28 X10^{-3} $(\Omega cm)^{-1}$ and 2.3X 10^{-5} $(\Omega cm)^{-1}$ respectively [39-40].

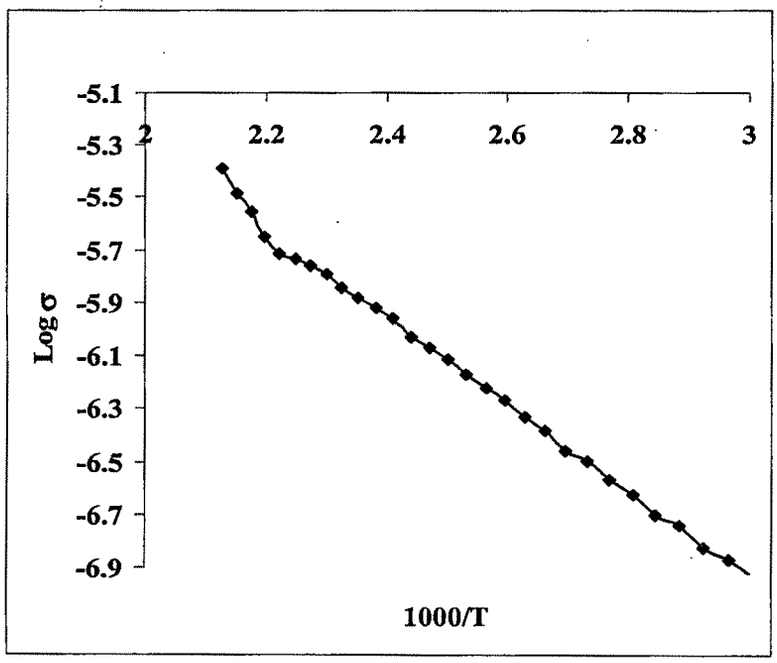

Fig 4.6 a (for x= 0.0)

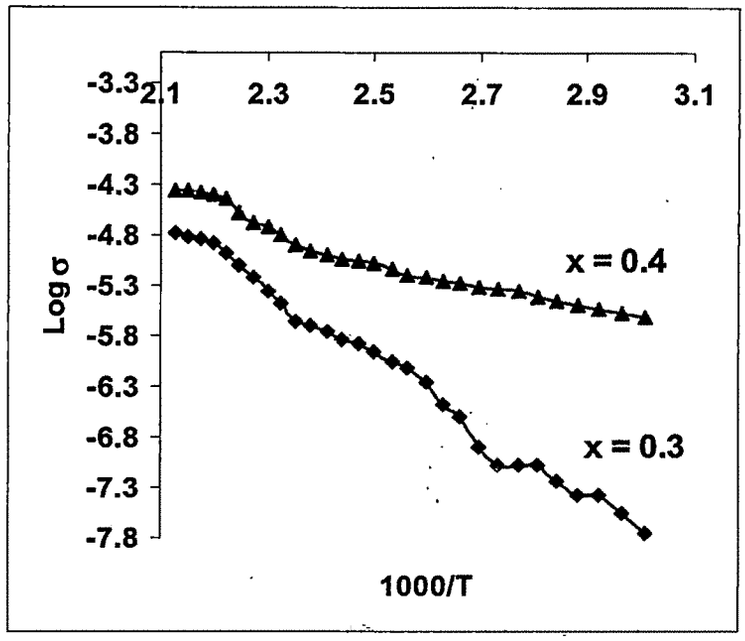

Fig 4.6 b & c

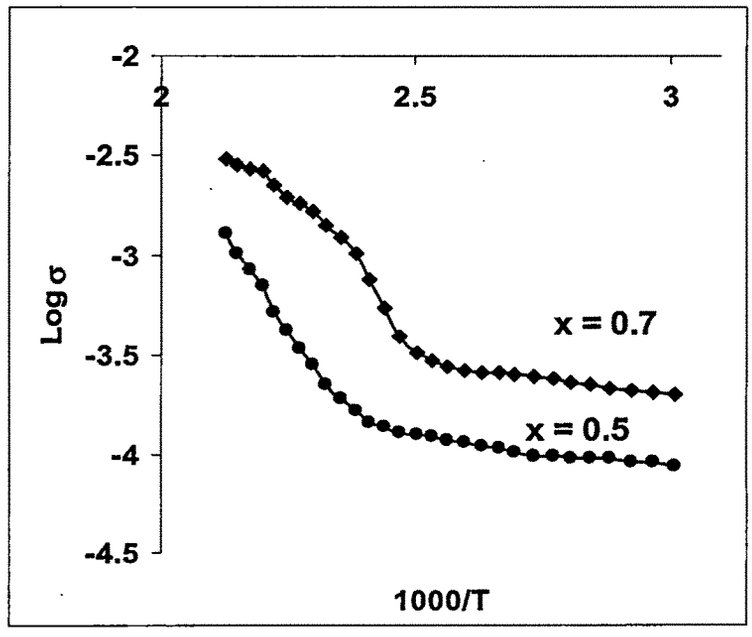

Fig 4.6 d & e

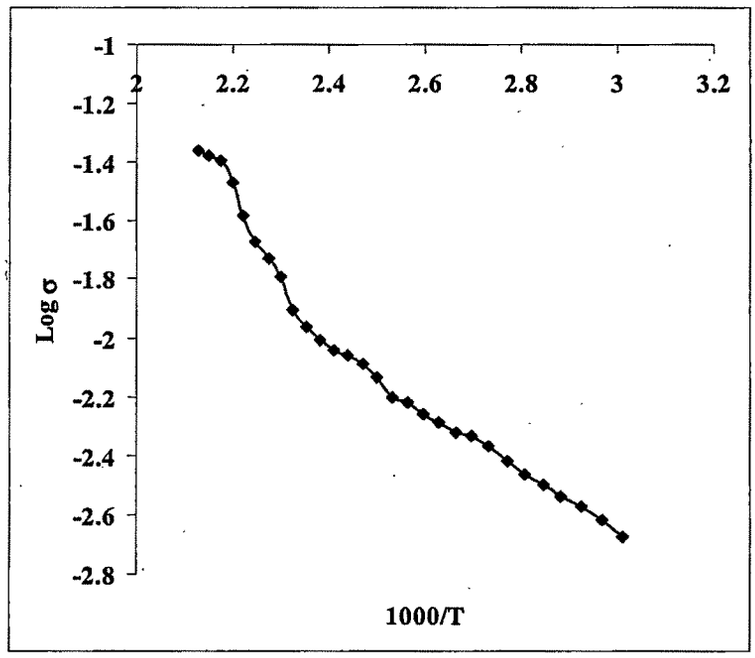

Fig.4.6 (f)

Fig 4.6: Plot of Log s versus 1000/T for chemically deposited $Cd_xPb_{1-x}S$ thin films for cadmium content, (a) x=0.0, (b) x=0.3, (c) x=0.4, (d) x=0.5, (e) x=0.7, (f) x=0.9.

4.7.2 Thermoelectric Power measurement

In TEP the type of conduction mechanism was examined by observing the nature of terminal connected to either positive or negative end. In our samples the negative terminal was connected to cold end indicating n type conductivity for all samples. The temperature dependence of TEP is shown in fig. 4.7. It is observed that the TEP increases upto x = 0.4 and thereafter decreases as composition parameter (x) increase from 0.5 to 1.

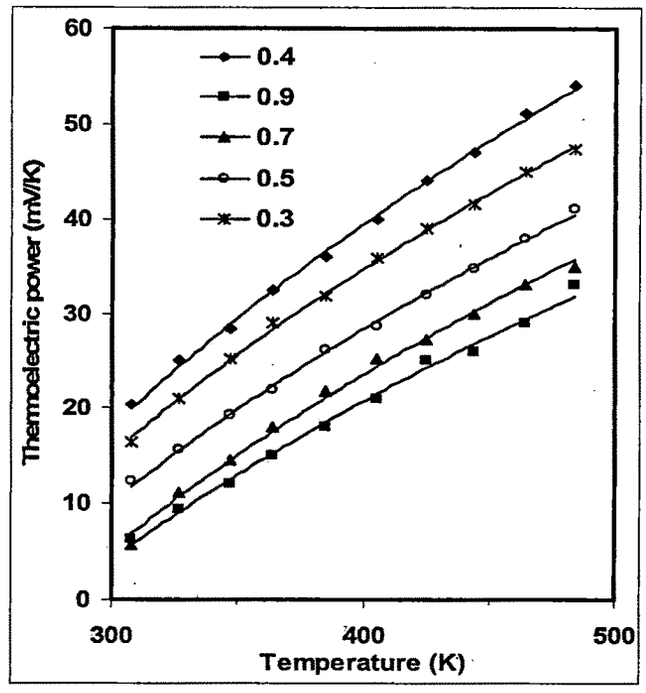

Fig. 4.7 Thermoelectric power measurements for chemically deposited $Cd_xPb_{1-x}S$ thin films

4.8 PEC characterization

The cell fabricated as described in 3.6.1 section of chapter 3 was used to study the charge transfer mechanism occurring across the semiconductor, electrolyte interface. The electrical characterization of the PEC cell was tested by studying I-V characteristics in dark, measurement of built in potential and power output characteristics.

4.8.1 Photoelectrical properties

4.8.1.1 Dynamic I-V characteristics in Dark

The (I-V) characteristics of the PEC have been studied at 303 K for bath, forwarded bias and reverse bias conditions. The ideality factor, n_d, is a measure of the junction quality and is determined from I-V characteristics in absence of light (dark). The ideal diode (Schottky Diode) equation assumes that all the recombination occurs via band to band or via traps in the bulk areas of the device (i.e. not in the junction) for which the ideality factor, n, is equal to one. As the energy level diagrams for both semiconductor-metal and semiconductor- electrolyte junctions are similar, therefore Schottky Diode equation of a semiconductor- metal junction is usually extended to

investigate semiconductor- electrolyte junction. The dynamic current voltage characteristics for films with composition x = 0.1, 0.4, 0.7 are shown in Fig. 4.8. The value of junction ideality factor were evaluated from the slope of the linear regions of the Log I_{sc} versus V variations [Fig. 4.9] and the values obtained for all the compositions are included in Table 5. It is seen that n_d value varies systematically with the photoelectrode composition(x). The n_d value were found to be higher than the ideal value (equal to one), a common fact found in many polycrystalline photo-electrode materials and is indication of the fact that the current transport across the interface has the influence of other kinds of recombination mechanism and series resistance effect, the former is due to presence of the surface states. The photoelectrode $Cd_{0.4}Pb_{0.6}S$ was shown to have the presence of least combination centers at the solid –liquid junction.

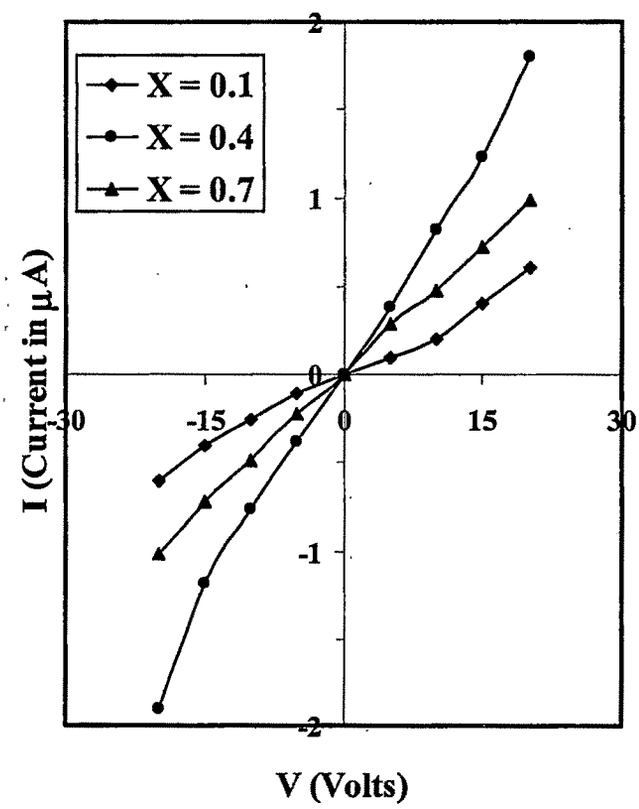

Fig 4.8 The dynamic current voltage characteristics for $Cd_xPb_{1-x}S$ films

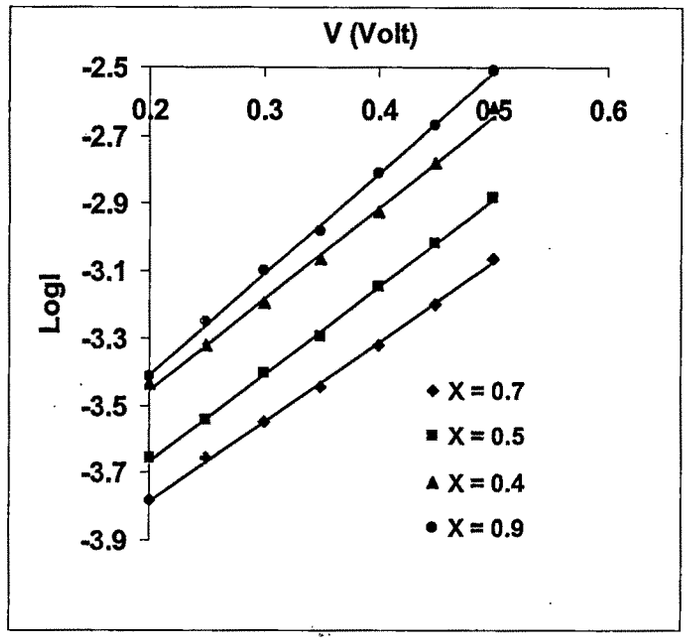

Fig 4.9: I-V Characteristics of few $Cd_x Pb_{1-x}S$ samples

4.8.1.2 Power output characteristics

A PEC cell may operate over a wide range of voltages and currents. By increasing the resistive load on a cell continuously from zero to a very high value (an open circuit), it is possible to determine the maximum-power point (i.e. the load for which the cell can deliver maximum electrical power). The energy conversion efficiency (η) of a cell is the percentage of power converted (from absorbed light to electrical energy) and collected and is given by;

$$[n = Pm / E \times Ac] \qquad (4.9)$$

where E is power of input light (in mW/cm^2) and A_c is the surface area of the cell in cm^2.

Another defining term in the overall behavior of a cell is the fill factor, which is the ratio of the maximum power (V_m x I_m) divided by the short-circuit current (I_{sc}) and open-circuit voltage (V_{oc}) in light current - voltage (I-V) characteristics of the cells.

The power output characteristics of few of the cells under a constant illumination of 40 mW/cm^2 is shown in Fig.4.10. The various cell

parameters like V_{oc}, I_{sc}, ff, η, have been determined and are included in Table 5.

It is observed that V_{oc} & I_{sc} have been boosted significantly at x = 0.4, but decreased thereafter. The increase in photocurrent in our case can be attributed to increase in band gap (from 1 eV to 1.5 eV), increased photosensitivity and improved grain quality that diminish series resistance of a cell. The SEM photographs (Figure 4.3) shows improvement in the grain boundaries upto X= 0.4, thereafter the grains become scare for higher values of x causing V_{oc} and I_{sc} to decrease. The Built in Potential, ϕ_b, can be determined by measuring the reverse saturation current (I_0) flowing through the junction at different temperatures. The values of built in potential were determined from the linear regions of $LogI_0/T^2$ versus 1/T plots and are included in Table 1. The nonlinearity of plots in high temperature regions can be attributed to Pool-Frankel type of conduction mechanism.

The observed conversion efficiencies are quite smaller due to i) strong absorption by the electrolyte material. ii) lack of post preparative treatments and iii) higher resistivity of the material.

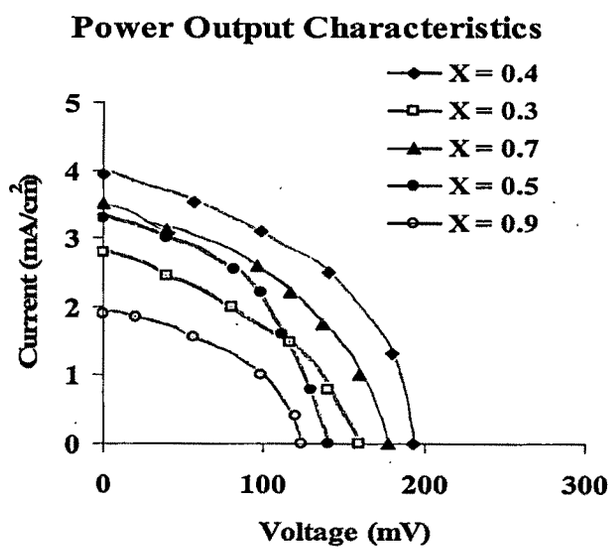

Fig. 4.10 Power output curves for representative $Cd_xPb_{1-x}S$ samples

4.9 Conclusions

The ternary solid solution $Cd_xPb_{1-x}S$ material in thin film form can be deposited by adopting the chemical bath deposition using Na_2EDTA as a complexing agent. The various properties of material obtained are measured and are given in this chapter.

The XRD analysis of annealed $Cd_xPb_{1-x}S$ thin films revealed that the solution containing lower concentration of Cd^{+2} ($x \leqslant 0.4$) forms solid solution of Cd^{+2} in PbS (cubic). Also the films with higher concentration of Cd^{+2} ($x \geqslant 0.5$) forms individual phases. From XRD data, values, of lattice parameter, grain size were calculated. The grain size calculated by scanning electron microscope agrees well with the particle size obtained form XRD.

As the compositional parameter 'x' increases the band gap increases from 0.8 eV to 2.4 eV. The specific conductance of $Cd_xPb_{1-x}S$ thin films at room temperature were found to be of the order of 10^{-3}-10^{-4} $(Ohmcm)^{-1}$. The activation energy of electrical conductivity was found to be of the order of 0.035 eV to 0.605 eV.

The TEP measurements reveal that the films behave like n-type semiconductors. In PEC the different cell performance parameters were studied with respect to the composition parameter (x). The photoanode film with x=0.4 composition shows better PEC performance characteristics.

Table 1: Compositional parameters of $Cd_xPb_{1-x}S$ thin films

Sr No	Composition	Bath content by calculation		Ratio of [Pb/Cd] in bath	Film content by AAS		Ratio of [Pb/Cd] on film	Thickness (in Å)
		Cd	Pb		Cd	Pb		
1.	PbS	-	1036	-	-		-	234
2.	$Cd_{0.1}Pb_{0.9}S$	57.2	932.4	16.300	11.4	186.4	16.35	227
3.	$Cd_{0.2}Pb_{0.8}S$	112.4	828.8	7.373	22.48	170.8	7.60	271
4.	$Cd_{0.3}Pb_{0.7}S$	168.65	725.2	4.303	33.73	153.2	4.54	201
5.	$Cd_{0.4}Pb_{0.6}S$	224.8	621.5	2.764	44.96	148.3	2.860	192
6.	$Cd_{0.5}Pb_{0.5}S$	281	518	1.834	56.2	103.6	1.843	283
7.	$Cd_{0.6}Pb_{0.4}S$	337	414	1.228	67.4	87.8	1.302	277
8.	$Cd_{0.7}Pb_{0.3}S$	392.5	310	0.7818	78.5	63	0.802	261
9.	$Cd_{0.8}Pb_{0.2}S$	449.5	207	0.4605	89.9	42.3	0.4705	243
10	$Cd_{0.9}Pb_{0.1}S$	505	103.6	0.2051	101	21.2	0.2099	218
11.	CdS	572	-	-	114.1	-	-	209

Table 2: Crystallographic parameters of $Cd_xPb_{1-x}S$ thin films

Film composition	d- Standard in Å		d- Observed in Å		hkl planes	
	PbS(C)	CdS(H)	PbS(C)	CdS(H)	PbS(C)	CdS(H)
PbS	3.429	-	3.4165	-	111	-
	2.969	-	2.9655	-	200	-
	2.099	-	2.0959	-	220	-
	1.790	-	1.7874	-	311	-
	1.714	-	1.7086	-	222	-
	1.484	-	1.4969	-	400	-
	1.327	-	1.3273	-	420	-
$Cd_{0.1}Pb_{0.9}S$	3.429	-	3.4181	-	111	-
	2.969	-	2.9673	-	200	-
	2.099	-	2.0921	-	220	-
	1.790	-	1.7881	-	311	-
	1.714	-	1.7127	-	222	-
	1.327	-	1.4833	-	420	-
	1.212	-	1.2118	-	422	-

$Cd_{0.2}Pb_{0.8}S$	3.429	-	3.4271	-	111	-
	2.969	-	2.9674	-	200	-
	2.099	-	2.0963	-	220	-
	1.790	-	1.7915	-	311	-
	1.714	-	1.7152	-	222	-
	1.484	-	1.4935	-	400	-
	1.327	-	1.3029	-	420	-
$Cd_{0.3}Pb_{0.7}S$	3.429	-	3.4280	-	111	-
	2.969	-	2.9684	-	200	-
	2.099	-	2.0936	-	220	-
	1.790	-	1.7887	-	311	-
	1.714	-	1.7134	-	222	-
	1.327	-	1.3251	-	420	-
	1.212	-	1.2088	-	422	-
$Cd_{0.4}Pb_{0.6}S$	3.429	-	3.4262	-	111	-
	2.969	-	2.9698	-	200	-
	2.099	-	2.0975	-	220	-
	1.790	-	1.7926	-	311	-
	1.714	-	1.7157	-	222	-
	1.484	-	1.489	-	400	-
	1.212	-	1.2179	-	420	-
$Cd_{0.5}Pb_{0.5}S$	3.429	3.583	3.4152	-	111	-
	2.969	3.357	2.9581	3.427	200	002
	2.099	3.160	2.0988	2.9583	220	101
	1.790	2.450	1.7851	2.4857	311	102
	1.714	2.068	1.7084	2.090	222	110
	1.484	1.791	1.4774	1.7858	400	200
		1.327		1.3242		211
		1.224		1.2082		204
		1.158		1.1390		213
$Cd_{0.6}Pb_{0.4}S$	3.429	3.583	3.4321	3.558	111	100
	2.969	3.357	2.9673	3.398	200	002
	2.099	3.160	2.0916	3.142	220	101
	1.790	2.450	1.7890	2.441	311	102
		2.068		2.065		110
		1.896		1.893		103
		1.791		1.731		200
		1.761		1.752		112
		1.581		1.553		202
$Cd_{0.7}Pb_{0.3}S$	3.429	3.357	3.445	3.331	111	002
	2.969	3.160	2.9552	3.153	200	101
	2.099	2.450	2.092	2.438	220	102
		2.068		2.059		110
		1.896		1.857		103
		1.761		1.740		112

$Cd_{0.8}Pb_{0.2}S$	3.429 2.099 1.790	3.357 3.160 2.450 2.068 1.896 1.581	3.440 2.902 1.732	3.326 3.140 2.440 2.071 1.903 1.605	111 200 311	002 101 102 110 103 202
$Cd_{0.9}Pb_{0.1}S$	3.429 2.969 1.790	3.357 3.160 2.450 2.068 1.896 1.791	3.4156 2.991 1.7132	3.330 3.192 2.495 2.271 1.932 1.805	111 200 220	002 101 102 110 103 200
CdS	- - - - - -	3.357 3.160 2.450 2.068 1.879 1.791	- - - - - -	3.3032 2.9578 2.4754 2.0751 1.8951 1.8250	- - - - - -	002 101 102 110 103 200-

Table 3 : Cell parameters, grain size of $Cd_xPb_{1-x}S$ thin films

Sr. No	Composition	Cell parameter (Å)			Grain size Å
		PbS a	CdS a	CdS c	XRD
1.	PbS	5.924	-	-	234
2.	$Cd_{0.1}Pb_{0.9}S$	5.920	-	-	240
3.	$Cd_{0.2}Pb_{0.8}S$	5.919	-	-	253
4.	$Cd_{0.3}Pb_{0.7}S$	5.900	-	-	259
5.	$Cd_{0.4}Pb_{0.6}S$	5.891	-	-	263
6.	$Cd_{0.5}Pb_{0.5}S$	5.925	4.2782	6.6064	520
7.	$Cd_{0.6}Pb_{0.4}S$	5.932	4.2157	6.5912	525
8.	$Cd_{0.7}Pb_{0.3}S$	5.910	4.3105	6.6101	537
9.	$Cd_{0.8}Pb_{0.2}S$	5.915	4.1903	6.633	525
10.	$Cd_{0.9}Pb_{0.1}S$	5.900	4.1512	6.703	570
11.	CdS	-	4.1315	6.722	600

Table: 4: Band gaps and activation energies of $Cd_xPb_{1-x}S$ thin films

Sr. No.	Composition	Band gap (eV)		Activation energy (eV)	
		PbS	CdS	HT	LT
1.	PbS	0.95	-	0.166	0.035
2.	$Cd_{0.1}Pb_{0.9}S$	1.01	-	0.201	0.073
3.	$Cd_{0.2}Pb_{0.8}S$	1.15	-	0.215	0.085
4.	$Cd_{0.3}Pb_{0.7}S$	1.2	-	0.233	0.097
5.	$Cd_{0.4}Pb_{0.6}S$	1.5	-	0.240	0.110
6.	$Cd_{0.5}Pb_{0.5}S$	1.1	2.24	0.415	0.135
7.	$Cd_{0.6}Pb_{0.4}S$	1.05	2.28	0.460	0.155
8.	$Cd_{0.7}Pb_{0.3}S$	1.0	2.24	0.527	0.170
9.	$Cd_{0.8}Pb_{0.2}S$	0.98	2.35	0.561	0.181
10.	$Cd_{0.9}Pb_{0.1}S$	-	2.4	0.573	0.189
11.	CdS	-	2.40	0.605	0.201

Table 5: Various photoelectrochemical parameters of $Cd_xPb_{1-x}S$ thin films

Composition (x)	Isc (mA)	Voc (V)	Im (mA)	Vm (V)	n	ff	nd	Φ_b
0	1.2	125	1.1	70	0.26	51.33	9.1	0.4
0.1	2	110	1.2	85	0.34	46.36	7.6	0.42
0.2	2.1	122	1.3	95	0.41	48.20	7.5	0.44
0.3	3.5	178	2.5	100	0.83	40.13	7.2	0.45
0.4	3.95	193	2.49	140	1.16	45.73	6.23	0.49
0.5	3.3	140	2.2	98	0.72	46.67	6.51	0.46
0.6	3.3	180	1.8	112	0.67	33.94	6.31	0.44
0.7	2.8	160	1.85	100	0.62	41.29	7.16	0.42
0.8	3.6	190	1.99	121	0.80	35.20	9.85	0.41
0.9	2.7	150	1.6	128	0.68	50.57	13.4	0.39
1	1.89	123	1.3	80	0.35	44.74	14.1	0.35

References

1] A. J. Varkey, Solar Energy Mater. 19(1989) 415.

2] I. I. Yu, T. Isobe, M. Serma, Mater.Res. Bull. 30 (1995)975.

3] G. Sauer, G. Berhm, S. Schneider, K. Nielsch, R. B. Wehrspohn, J. Choi, H. Hofmeister, U. Gosele, J. Appl. Phys. 91 (2002) 3242.

4] G. P. Kotiyal, B. Ghosh, R. Y. Deshpande, J. Phys. D 13 (1980) 869.

5] T. Tohma, H. Masumoto, T. Goto, Jpn. J. Appl. Phys. Part 14 (IIB) (2002) 6643.

6] A. Dixit, S. B. Majumdar, R. S. Katiyar, A. S. Bhalla, Appl. Phys. Lett. 82 (6) (2003) 2679.

7] V. B. Patil, G. S. Shahane, D. S. Sutrave, B.T. Raut, L.P. Deshmukh, Thin solid Films, 446(2004)1.

8] H. Unuma, Y. Saito, K. Watanabe, M. Sugawara, Thin solid Films, 468(2004) 4.

9] P. J. George, A. Sanchez, P. K. Nair, L. Huang, J. Crystal Growth, 158 (1996) 53.

10] H. Weller, Angew. Chem. Int. Ed. Engl. 105 (1993) 41.

11] A. L. Saligson, J. Arnold, J. Am. Chem. Soc. 116 (1993) 8214.

12] A. C. Rastogi, K. S. Balkirshnan, A. Garg, J. Electrochem. Soc. 140 (1993) 2373.

13] A. I. Vogel, "A Textbook of Quantitative Inorganic Analysis", 4th Ed. Longman Inc, New York (1978).

14] A. E. Nielsen, "Kinetics of Precipitation", Pergamon Press, Oxford (1964).

15] J. A. Venables, "Introduction to Surface and Thin Film Processes", Cambridge University, Press (2000).

16] R. A. Boudreau, R. D. Rauh, J. Electrochem. Soc. 130 (1983)573.

17] G. A. Kitaev, S. G. Mokrushin, A. A. Uritskaya, Colloid. J. USSR, 27 (1965) 38.

18] A. B. Lundin, G.A. Kitaev, Inorg. Mater. 1 (1965)2107.

19] O. Brien, P. J. McAleese, J. Mater. Chem. 8 (1998) 2309.

20] G. K. Padam, Thin Solid Films 150(1987) L89.

21] G. S. Morris, R. Vanderveen, Solar Energy Mater. Sol. Cells 27 (1992) 305.

22] I. O. Oladegi, L. Chow, J. Electrochem. Soc. 144 (1997)2342.

23] M. J. Mangalam, K. N.Rao, N. Rangarajan, C. V. Suryanaryana, J. Appl. Phys. 7 (1969) 629.

24] N. Romeo, A. Boiso, R. Tedeschi, V. Canevari, Mater. Chem. Phys. 66 (2000) 201.

25] Feliciano Sanchez-Sinencio, J. G. Mendoza, -Alvarez, O. Zelaya, Alberto Herrera, Francisco Larios, Thin solid Films, 193/194(1990)382.

26] G. H. Aylward, T. J. V. Findlay, "SI Chemical Data", 113 Wiley, Melbourne, (1974).

27] H. N. Acharya, H .N. Bose, Phys. Stat. Sol. (1973) K-43.

28] K. M. Gadave, S. A. Jodgudri, C. D. Lokhande, Thin Solid Films, 245 (1994) 7.

29] P. K. Nair, m. T. S. Nair, Semicond. Sci. Technol. 4 (1989) 807.

30] B. Pradhan, A. K. Sharma, A. K. Ray, Journal of Crystal Growth, Volume 304, Issue 2,(2007) 388.

31] E. Çetinörgü, C. Gümü , R. Esen, Thin Solid Films, Volume 515, Issue 4, (2006)1688.

32] JCPDS Card No. G-0314.

33] JCPDS Card No. 05-0592

34] L. P. Deshmukh, s. G.Hollikatti, P. P. Hankare, Bull. Mater. Sci. 17 (1994) 455.

35] N. F. foster, J. Appl. Phys. 38 (1968) 149.

36] Cristina Nascu,Valentina Vomir, Ileana Pop,Violeta Ionescu and Rodica Grew, Mater. Sci. & Eng. B 41 (1996) 235.

37] B. Pradhan, A. K. Sharma, A. K. Ray, Journal of Crystal Growth, Volume 304, Issue 2, (2007), 388.

38] Azaroff, "Introduction to Solids", Academic Press, New York (1960) 222.

39] L. Smart, E. Moore, "Solid State Chemistry: An Introduction 2nd "(Eds) Cheltenham: Stanley Thornes (Publishers) Ltd. (1998)382.

40] S. Abe. K. Masumoto, K. Suto , Journal of Crystal Growth 181 (1997) 367.

41] P.K. Nair, V.M.Garcia, A.B.Hernandez, M.T. S. Nair, Journal of Physics D, 24(1991) 1466.